Chemical Science

ROYAL SOCIETY
OF CHEMISTRY

EDGE ARTICLE

Check for updates

Integration of exonuclease III-powered three-dimensional DNA walker with single-molecule detection for multiple initiator caspases assay†

Meng Liu,‡[a] Rui Xu,‡[a] Wenjing Liu,‡[b] Jian-Ge Qiu,*[b] Yan Wang,*[a] Fei Ma*[c] and Chun-yang Zhang [ID] *[a]

Initiator caspases are important components of cellular apoptotic signaling and they can activate effector caspases in extrinsic and intrinsic apoptotic pathways. The simultaneous detection of multiple initiator caspases is essential for apoptosis mechanism studies and disease therapy. Herein, we develop a sensitive nanosensor based on the integration of exonuclease III (Exo III)-powered three-dimensional (3D) DNA walker with single-molecule detection for the simultaneous measurement of initiator caspase-8 and caspase-9. This assay involves two peptide–DNA detection probe-conjugated magnetic beads and two signal probe-conjugated gold nanoparticles (signal probes@AuNPs). The presence of caspase-8 and caspase-9 can induce the cleavage of peptides in two peptide–DNA detection probes, releasing two trigger DNAs from the magnetic beads, respectively. The two trigger DNAs can serve as the walker DNA to walk on the surface of the signal probes@AuNPs powered by Exo III digestion, liberating numerous Cy5 and Texas Red fluorophores which can be quantified by single-molecule detection, with Cy5 indicating caspase-8 and Texas Red indicating caspase-9. Notably, the introduction of the AuNP-based 3D DNA walker greatly reduces the background signal and amplifies the output signals, and the introduction of single-molecule detection further improves the detection sensitivity. This nanosensor is very sensitive with a detection limit of 2.08×10^{-6} U μL^{-1} for caspase-8 and 1.71×10^{-6} U μL^{-1} for caspase-9, and it can be used for the simultaneous screening of caspase inhibitors and the measurement of endogenous caspase activity in various cell lines at the single-cell level. Moreover, this nanosensor can be extended to detect various proteases by simply changing the peptide sequences of the detection probes.

Introduction

Apoptosis is programmed cell death which can result in the disappearance of cells without any inflammatory phenomena.[1] Caspases are a family of cysteinyl aspartate-directed proteases, and they are the central executioners of apoptosis.[2] Once activated by a specific stimulus (*e.g.*, ultraviolet (UV) radiation, γ-irradiation, heat, DNA damage, viral virulence factors),[3]

[a]College of Chemistry, Chemical Engineering and Materials Science, Collaborative Innovation Center of Functionalized Probes for Chemical Imaging in Universities of Shandong, Key Laboratory of Molecular and Nano Probes, Ministry of Education, Shandong Provincial Key Laboratory of Clean Production of Fine Chemicals, Shandong Normal University, Jinan 250014, China. E-mail: cyzhang@sdnu.edu.cn; fagong@sdu.edu.cn; Fax: +86-0531-82615258; Tel: +86-0531-86186033

[b]Academy of Medical Sciences, The Affiliated Cancer Hospital of Zhengzhou University, Zhengzhou University, Zhengzhou, 450000, China. E-mail: jiangeqiu@zzu.edu.cn

[c]School of Chemistry and Chemical Engineering, Southeast University, Nanjing, 211189, China. E-mail: fei@seu.edu.cn

† Electronic supplementary information (ESI) available. See DOI: 10.1039/d1sc05115f

‡ These authors contributed equally to this work.

caspases execute the part-proteolysis of downstream substrates to trigger a cascade of events that culminates in the desired biological response: disruption of cellular membranes, breaking down of cytoplasmic and nuclear skeletons, extruding of cytosol, degradation of chromosomes, and fragmentation of the nucleus.[4] Inappropriate apoptosis and deregulation of caspase activity are implicated in various human diseases, including Alzheimer's disease,[5] ischemic damage,[6] autoimmune diseases,[7] and cancers.[8] The apoptotic-associated caspases are classified into initiators and effectors by their location in the apoptosis cascade signalling pathways. The initiator caspases (*e.g.*, caspase-8, caspase-9, and caspase-10) are responsible for initiating the apoptosis cascade, and the effector caspases (*e.g.*, caspase-3, caspase-6, and caspase-7) can be activated by initiator caspases to destroy cellular proteins and execute apoptosis.[9] Extrinsic and intrinsic apoptotic pathways are the only two pathways of apoptosis, and caspase-8 and caspase-9 are critical participants in extrinsic and intrinsic apoptosis, respectively. In the extrinsic apoptotic pathway, caspase-8 is specifically activated by death receptors such as Fas/CD95.[10] In the intrinsic apoptotic pathway, caspase-9 is

activated by the accumulation of cytochrome C in the cytosol due to dissipation of the mitochondrial membrane potential.[11] Therefore, the simultaneous measurement of caspase-8 and caspase-9 are of great importance for the study of the apoptosis mechanism and disease therapy.

Conventional methods for caspase assays include enzyme-linked immune sorbent assay (ELISA),[12] western blot,[13] flow cytometry,[14] and mass spectrometry.[15] They usually involve multi-step and time-consuming processes,[16] and extensive pre-treatment of samples.[17] Recently, a variety of new methods have been developed for *in vitro* and *in vivo* detection of cas-pases, including electrochemical,[18] colorimetric[19] and fluores-cence measurements.[20,21] Most of these methods rely on either antibodies[18] or peptide substrates.[19–21] The main limitation of antibody-based assays is the requirement for high quality antibodies.[22] Alternatively, peptide substrates are a more attractive choice for caspase assay with the distinct advantages of accessibility, simplicity, cost-effectiveness, and chemical definition.[23] In the peptide substrate-based assays, peptide substrates are often labelled with fluorophores and the fluo-rescence signals are directly measured after caspase cleavage, resulting in limited sensitivity.[24] The development of new methods for sensitive caspase assay is highly desirable.

Due to the highly selective and programmable Watson–Crick complementarity, DNA is becoming an increasingly attractive building material for the construction of a series of functional nanodevices (*e.g.*, walker,[25–27] gear,[28] and tweezer[29]). In partic-ular, a DNA walker that is able to convert chemical energy to mechanical motion is the most widely studied DNA nanodevice and has been extensively applied for molecular transport,[30] DNA computing,[31] chemical synthesis,[32] and biosensing.[33,34] DNA walkers can be classified into one-dimensional (1D), two-dimensional (2D), and three-dimensional (3D) DNA walkers in terms of dimensionality. The 1D DNA walkers move along 1D tracks such as double-stranded DNA (dsDNA) and single walled carbon nanotubes (SWCNTs).[35,36] 2D DNA walkers can move along the 2D surfaces of gold electrodes and DNA tile.[37,38] 3D DNA walkers can move along 3D scaffolds on nanoparticles such as gold nanoparticles (AuNPs),[39] magnetic beads (MBs),[40] SiO$_2$@CdTe,[41] Au@Fe$_3$O$_4$,[42] hollow carbon nanospheres (HCS),[43] and DNA origami.[44] Such 3D DNA walkers are usually powered by nicking endonucleases,[45,46] exonuclease III (Exo III),[47] or the DNA catalytic hairpin assembly reaction,[48] and possess large specific surface area and high DNA loading capability,[49] and they can greatly enhance the local concentra-tion of track DNA for improved walking efficiency and higher processivity,[50] facilitating high signal gain in a given period of time.[51]

A rolling circle amplification (RCA)-based method has been developed for caspase assay,[52] but it is only suitable for single target detection and is prone to a high background due to nonspecific amplification. In addition, it requires laborious procedures for the preparation of the circular template, and its accuracy is challenged by the inner filter effect and the colli-sional quenching of ensemble fluorescence measurements. Herein, we develop a simple and sensitive caspase nanosensor with the capability of multiplexed assay based on the

integration of an Exo III-powered 3D DNA walker with single-molecule detection. The Exo III mediates highly efficient signal amplification through catalyzing the cyclic digestion of one strand of dsDNA from the 3′ end,[53] which can be performed under isothermal conditions with the elimination of complex thermal cycling and nonspecific artificial amplification involving in polymerase chain reaction (PCR).[54] In comparison with other isothermal amplification methods such as strand displacement amplification (SDA),[55] exponential amplification reaction (EXPAR),[56] rolling circle amplification,[57] and loop mediated isothermal amplification (LAMP),[58] the Exo III-mediated amplification takes advantage of a much simpler reaction scheme without the requirement of a specific recog-nition sequence for nicking endonuclease, complicated proce-dures for preparation of the circular template, and multiple primers for completing the amplification reaction. Moreover, in comparison with the ensemble measurement, single-molecule detection has the distinct advantages of high sensitivity, simplicity, and low sample consumption.[59–65] This assay involves two peptide–DNA detection probe-conjugated magnetic beads and two signal probe-conjugated gold nano-particles (signal probes@AuNPs). The integration of Exo III-mediated amplification with the AuNP-based DNA walker facilitates facile and efficient amplification of the caspase signal to acquire high sensitivity with reduced background, and the introduction of single-molecule detection further improves the detection sensitivity. The presence of caspase-8 and caspase-9 can induce the cleavage of peptides in two peptide–DNA detection probes, releasing two trigger DNAs from the magnetic beads. The two trigger DNAs can serve as the walker DNA to walk on the surface of signal probes@AuNPs powered by Exo III digestion, liberating numerous Cy5 and Texas Red fluorophores which can be quantified by single-molecule detection, with Cy5 indicating caspase-8 and Texas Red indicating caspase-9. This nanosensor is very sensitive with a detection limit of 2.08×10^{-6} U μL^{-1} for caspase-8 and 1.71×10^{-6} U μL^{-1} for caspase-9, and it can be used for simultaneous screening of caspase inhibitors and measurement of endogenous caspase activity in various cell lines at the single-cell level. To the best of our knowledge, the integration of Exo III-powered 3D DNA walker with single-molecule detection for the simultaneous measure-ment of multiple caspases has not been explored so far.

Results and discussion

The schematic illustration of the nanosensor based on the integration of the Exo III-powered 3D DNA walker with single-molecule detection for the simultaneous measurement of initiator caspase-8 and caspase-9 is shown in Scheme 1. This assay involves two peptide–DNA detection probe-conjugated magnetic beads and two signal probe-conjugated gold nano-particles (signal probes@AuNPs). The biotinylated peptide–DNA detection probes (Fig. S1, ESI†) can be self-assembled on the streptavidin-coated MBs through the specific streptavidin–biotin interaction. The peptide domain of detection probe 1 (Scheme 1, green color) contains a tetrapeptide sequence Ile–Glu–Thr–Asp (IETD) for caspase-8 recognition, and the peptide
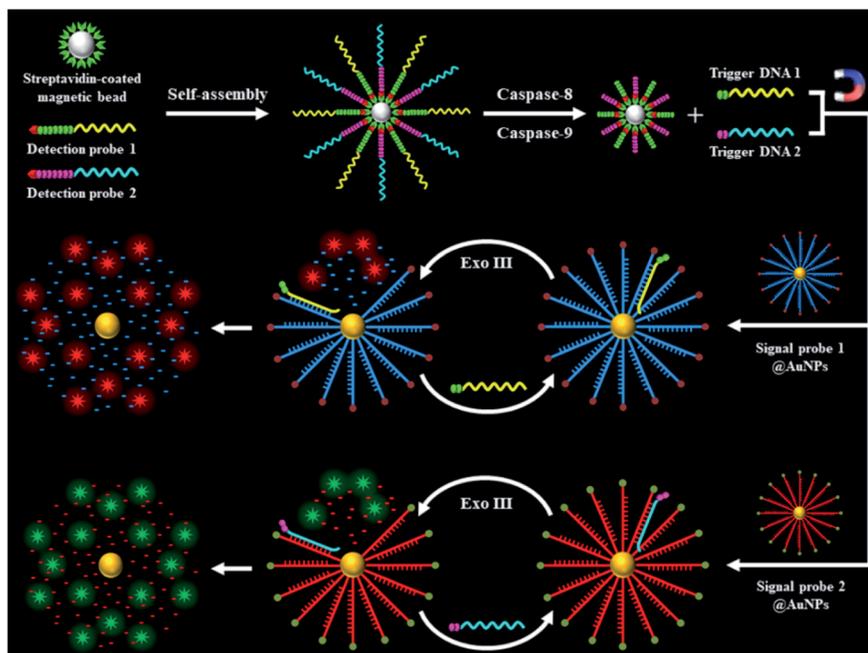
Scheme 1 Schematic illustration of the integration of Exo III-powered 3D DNA walker with single-molecule detection for the simultaneous measurement of initiator caspase-8 and caspase-9.

domain of detection probe 2 (Scheme 1, magenta color) contains a tetrapeptide sequence Leu–Glu–His–Asp (LEHD) for caspase-9 recognition. The DNA domain of detection probe 1 (Scheme 1, yellow color) is complementary to signal probe 1 (Scheme 1, blue color), and the DNA domain of detection probe 2 (Scheme 1, cyan color) is complementary to signal probe 2 (Scheme 1, red color). Signal probes are attached to the surface of AuNPs *via* a Au–S bond to form the 3D scaffold of the DNA walker which is powered by Exo III. In the presence of caspase-8, it specifically recognizes the sequence IETD and hydrolyzes the peptide bond adjacent to the carboxylic group of the aspartic acid residue (*i.e.*, the peptide bond between aspartic acid and glycine), releasing the cleaved detection probe 1 from the magnetic beads (Fig. S1A, ESI†). In the presence of caspase-9, it specifically recognizes the sequence LEHD and hydrolyzes the peptide bond between aspartic acid and glycine, releasing the cleaved detection probe 2 from the magnetic beads (Fig. S1B, ESI†). The intact detection probes are separated by magnetic separation. The trigger DNA in the cleaved detection probes (Scheme 1, yellow and cyan color) can serve as the walker DNA to initiate the recyclable cleavage of signal probes on the surface of the AuNPs, releasing numerous Cy5 and Texas Red fluorophores from the signal probes@AuNPs. Specifically, the hybridization of trigger DNA 1 of the cleaved detection probe 1 (Scheme 1, yellow color) and signal probe 1 (Scheme 1, blue color) form a dsDNA with 5′ overhangs, which can be recognized by Exo III. The stepwise catalytic removal of mononucleotides from the 3′-terminus of signal probe 1 (Scheme 1, blue color) leads to the liberation of the Cy5 fluorophore from the signal probe 1@AuNPs, while the digestion of trigger DNA 1 (Scheme 1, yellow color) is blocked by the oligo-T tail. As the digestion of signal probe 1 (Scheme 1, blue color) proceeds, the trigger DNA

1 (Scheme 1, yellow color) is partially released and hybridizes with another signal probe 1 (Scheme 1, blue color) nearby. In this way, the trigger DNA 1 (Scheme 1, yellow color) walks along the AuNP surface, and abundant Cy5 fluorophores are liberated from the signal probe 1@AuNPs, resulting in the restoration of Cy5 fluorescence which can be quantified by single-molecule detection, with Cy5 indicating the presence of caspase-8. Similarly, the hybridization of trigger DNA 2 of the cleaved detection probe 2 (Scheme 1, cyan color) with signal probe 2 (Scheme 1, red color) forms a dsDNA with 5′ overhangs, which can be recognized by Exo III. The Exo III-mediated stepwise catalytic removal of mononucleotides from the 3′-terminus of signal probe 2 (Scheme 1, red color) leads to the liberation of abundant Texas Red fluorophores from the signal probe 2@AuNPs, resulting in the restoration of Texas Red fluorescence which can be used for the quantification of caspase-9. Because there are 120 signal probes per AuNP (ESI†), the high density of the scaffold DNA enhances the movement of trigger DNA along the 3D tracks, greatly amplifying the fluorescence signals. In contrast, in the absence of caspase-8 and caspase-9, the detection probes remain intact, and no trigger DNA is released. Consequently, no Exo III-mediated digestion of signal probes occurs, and neither the Cy5 nor Texas Red signal can be detected.

This assay mainly relies on the caspase-mediated cleavage of peptide to initiate the recycling liberation of Cy5/Texas Red fluorescent molecules from the signal probes@AuNPs. We used 12% nondenaturing polyacrylamide gel electrophoresis (PAGE) to verify the cleavage of the detection probes by caspase-8 and caspase-9. For the caspase-8 assay, when caspase-8 is absent, only one distinct band is observed (Fig. 1A, lane 2), which is identical to that of the intact detection probe 1, indicating that
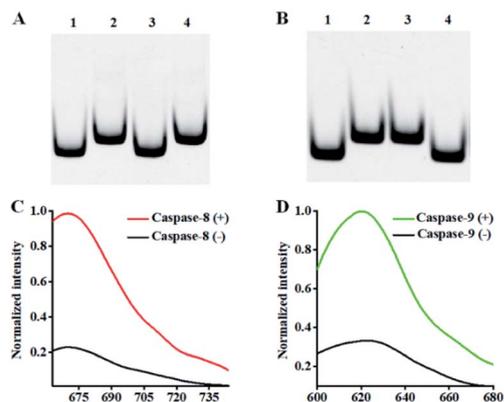
Fig. 1 (A) 12% nondenaturing PAGE analysis of caspase-8-mediated cleavage of detection probe 1. Lane 1: the synthesized cleaved peptide–DNA 1; lane 2: detection probe 1; lane 3: detection probe 1 + 0.025 U μL^{-1} caspase-8; lane 4: detection probe 1 + 0.025 U μL^{-1} caspase-9. (B) 12% nondenaturing PAGE analysis of the caspase-9-mediated cleavage of detection probe 2. Lane 1: the synthesized cleaved peptide–DNA 2; lane 2: detection probe 2; lane 3: detection probe 2 + 0.025 U μL^{-1} caspase-8; lane 4: detection probe 2 + 0.025 U μL^{-1} caspase-9. (C) Fluorescence measurements of the caspase-8-initiated recycled liberation of Cy5 molecules from the signal probe 1@AuNPs in the absence (black line) and presence (red line) of caspase-8. (D) Fluorescence measurements of the caspase-9-initiated recycling liberation of Texas Red molecules from the signal probe 2@AuNPs in the absence (black line) and presence (green line) of caspase-9. The 0.025 U μL^{-1} caspase-9 and 0.5 U of Exo III were used in the experiments.

the cleavage of detection probe 1 cannot occur in the absence of caspase-8. When caspase-8 is present, a new smaller-sized band is observed (Fig. 1A, lane 3), which corresponds to the cleaved peptide–DNA 1 (Fig. 1A, lane 1), indicating the cleavage of detection probe 1 induced by caspase-8. When only caspase-9 is present, only one identical band to that of the intact detection probe 1 (Fig. 1A, lane 2) is observed (Fig. 1A, lane 4), indicating that the cleavage of detection probe 1 cannot occur in the presence of caspase-9. For the caspase-9 assay, when caspase-9 is absent, only one distinct band is observed (Fig. 1B, lane 2), which is identical to that of intact detection probe 2, indicating that the cleavage of detection probe 2 cannot occur in the absence of caspase-9. When only caspase-8 is present, only one distinct band identical to lane 2 (Fig. 1B) is observed (Fig. 1B, lane 3), indicating that the cleavage of detection probe 2 cannot occur in the presence of caspase-8. When caspase-9 is present, a new smaller-sized band is observed (Fig. 1B, lane 4), which corresponds to the cleaved peptide–DNA 2 (Fig. 1B, lane 1), indicating the cleavage of detection probe 2 induced by caspase-9. To verify the feasibility of the proposed nanosensor, we performed fluorescence measurements (Fig. 1C and D). As shown in Fig. 1C, a distinct Cy5 fluorescence signal with a characteristic emission peak of 670 nm is observed in the presence of 0.025 U μL^{-1} caspase-8 (Fig. 1C, red line). In contrast, in the control group without caspase-8, a low Cy5 signal (Fig. 1C, black line) is detected. As shown in Fig. 1D, a distinct Texas Red fluorescence signal with a characteristic emission peak of 620 nm is observed in the presence of 0.025 U μL^{-1} caspase-9

(Fig. 1D, green line). In contrast, in the control group without caspase-9, a low Texas Red signal (Fig. 1D, black line) is detected.

We further employed single-molecule detection technology to detect the fluorescence signals (Fig. 2). In the absence of caspase-8 and caspase-9, neither Cy5 (Fig. 2A) nor the Texas Red fluorescence signal (Fig. 2E) is observed, indicating that the Exo III-mediated recycling liberation of fluorophores cannot occur in the absence of caspase-8 and caspase-9. In contrast, in the presence of 0.025 U μL^{-1} caspase-8, distinct Cy5 fluorescence signals are observed (Fig. 2B, red color), but no Texas Red fluorescence signal is detected (Fig. 2F), indicating that caspase-8 can induce the recycling liberation of Cy5 fluorophores from the signal probe 1@AuNPs. In the presence of 0.025 U μL^{-1} caspase-9, distinct Texas Red fluorescence signals are observed (Fig. 2G, green color), but no Cy5 fluorescence signal is detected (Fig. 2C), indicating that caspase-9 can induce the recycling liberation of Texas Red fluorophores from the signal probe 2@AuNPs. In the presence of both caspase-8 and caspase-9, distinct Cy5 (Fig. 2D, red color) and Texas Red fluorescence signals (Fig. 2H, green color) are simultaneously observed. Notably, both the Cy5 and Texas Red fluorescence spots exhibit single-step photobleaching (Fig. S3, ESI†), suggesting that the observed individual fluorescent spot originates from a single dye molecule. These results clearly demonstrate that the proposed nanosensor can be applied for the simultaneous detection of caspase-8 and caspase-9 at the single-molecule level.

Under the optimized experimental conditions (Fig. S4 and S5, ESI†), we evaluated the sensitivity of the proposed nanosensor by measuring the variance of fluorescent counts with the caspase concentration. As shown in Fig. 3A, the Cy5 counts improve with increasing concentration of caspase-8 from 2.50×10^{-6} to 0.05 U μL^{-1}. In the logarithmic scale, the Cy5 counts show a linear correlation with the concentration of caspase-8 over the range from 2.50×10^{-6} to 2.50×10^{-3} U μL^{-1}. The regression equation is $N = 510.06 + 89.12 \log_{10} C$ with a correlation coefficient (R^2) of 0.9990 (inset of Fig. 3A), where N is the
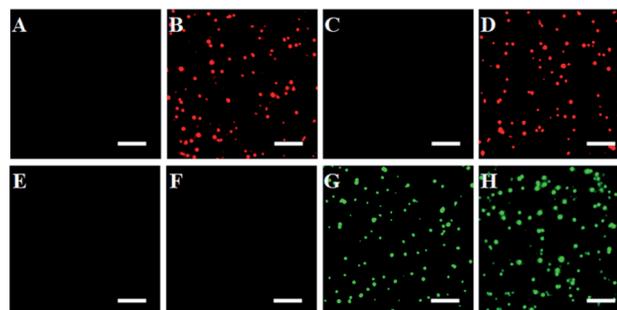

Fig. 2 Simultaneous detection of multiple caspases by single-molecule imaging in the absence (A and E) and presence of caspase-8 (B and F), caspase-9 (C and G), and caspase-8 + caspase-9 (D and H). The Cy5 fluorescence signals are shown in red, and the Texas Red fluorescence signals are shown in green. The 0.025 U μL^{-1} caspase-8, 0.025 U μL^{-1} caspase-9 and 0.5 U of Exo III were used in the experiments. The scale bar is 4 μm.
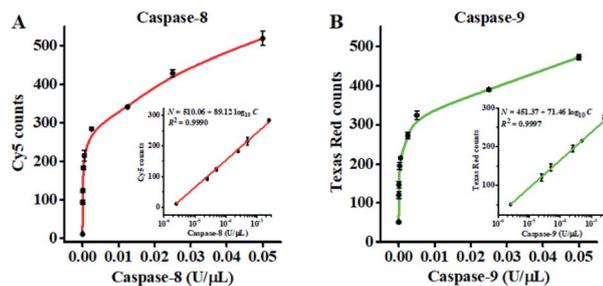
Fig. 3 (A) Measurement of Cy5 counts generated by different concentrations of caspase-8. The inset shows the linear relationship between the Cy5 counts and the logarithm of caspase-8 concentration. (B) Measurement of Texas Red counts generated by different concentrations of caspase-9. The inset shows the linear relationship between the Texas Red counts and the logarithm of caspase-9 concentration. The 0.5 U of Exo III was used in the experiments. Error bars represent the standard deviation of three experiments.

measured Cy5 count and C is the concentration of caspase-8 (U μL^{-1}). By evaluating the average response of the control group plus three times the standard deviation, the limit of detection (LOD) was calculated to be 2.08×10^{-6} U μL^{-1} (7.51 pM). The sensitivity of the proposed nanosensor is 96-fold higher than the conjugated polymer-based fluorescence assay (0.2 U mL^{-1}),[66] and 439-fold higher than the reported fluorescence assay (3.3 nM).[67]

As shown in Fig. 3B, the Texas Red counts improve with increasing concentration of caspase-9 from 2.50×10^{-6} to 0.05 U μL^{-1}. In the logarithmic scale, the Texas Red counts show a linear correlation with the concentration of caspase-9 over a range from 2.50×10^{-6} to 2.50×10^{-3} U μL^{-1}. The regression equation is $N = 451.37 + 71.46 \log_{10} C$ with a correlation coefficient (R^2) of 0.9997 (inset of Fig. 3B), where N is the measured Texas Red count and C is the concentration of caspase-9 (U μL^{-1}). The LOD was calculated to be 1.71×10^{-6} U μL^{-1} (92.37 pM). The sensitivity of the proposed nanosensor is 40-fold higher than the up-conversion nanoparticles-based FRET assay (0.068 U mL^{-1}),[68] and 650-fold higher than the gold nanoparticle–polydopamine-based electrochemical immunosensor (0.06 μM).[18] The improved sensitivity of the proposed nanosensor can be ascribed to (1) the efficient conversion of the caspase activity signal into the DNA signal through the cleavage of the peptide–DNA detection probe, (2) recyclable liberation of fluorescent molecules from the signal probes@AuNPs induced by the Exo III-driven 3D DNA walker, and (3) the high signal-to-noise ratio of single-molecule detection.

To investigate the selectivity of the proposed nanosensor for caspase assay, we used caspase-3, DNA (cytosine-5)-methyltransferase 1 (Dnmt1) and human alkyladenine DNA glycosylase (hAAG) as the negative controls. Caspase-3 is a core effector caspase that can be activated by caspase-8 in the extrinsic apoptotic pathway and can be activated by caspase-9 in the intrinsic pathway, but it cannot cleave the peptide substrates of caspase-8 and caspase-9.[16] Dnmt1 can specifically recognize the hemimethylated sequence 5′-CG-3′, and catalyze the transfer of a methyl group from S-adenosyl-L-methionine

(SAM) to the cytosine in genomic DNA.[69] hAAG can recognize and excise a diverse group of alkylated purine bases and cleave the N-glycosidic bond between the sugar and the damaged base.[70] As shown in Fig. 4, in the presence of caspase-3, Dnmt1 and hAAG, neither Cy5 nor Texas Red fluorescence signal is observed, consistent with the control with only the reaction buffer. In contrast, in the presence of caspase-8, an enhanced Cy5 fluorescence signal is observed, but no Texas Red fluorescence signal is detected. In the presence of caspase-9, an enhanced Texas Red fluorescence signal is detected, but no Cy5 fluorescence signal is detected. Moreover, in the presence of both caspase-8 and caspase-9, both Cy5 and Texas Red fluorescence signals can be simultaneously detected. These results demonstrate that the proposed nanosensor exhibits excellent selectivity toward caspase-8 and caspase-9.

To investigate the feasibility of the proposed nanosensor for kinetic analysis, we measured the initial velocity (V) in response to various concentrations of the detection probes. To evaluate the enzyme kinetic parameters of caspase-8, we measured the V in the presence of 0.025 U μL^{-1} caspase-8 and different concentrations of detection probe 1 for 5 min at 37 °C. As shown in Fig. 5A, the initial velocity of caspase-8 enhances with the increasing concentration of detection probe 1. V_{max} is calculated to be 146.55 min^{-1} and K_m is calculated to be 1.39 μM. The K_m value is consistent with that obtained by the rolling circle amplification (RCA)-based fluorescence assay (1 μM).[52] To evaluate the enzyme kinetic parameters of caspase-9, we measured the V in the presence of 0.025 U μL^{-1} caspase-9 and different concentrations of detection probe 2 for 5 min at 37 °C. As shown in Fig. 5B, the initial velocity of caspase-9 enhances with the increasing concentration of detection probe 2. V_{max} is calculated to be 109.12 min^{-1} and K_m is calculated to be 1.21 μM. The K_m value is consistent with that obtained by the multicolor gold–selenium bonding nanoprobe-based fluorescence assay (8.53 μM).[71] These results suggest that the proposed nanosensor can be used to accurately evaluate the kinetic parameters of caspases.
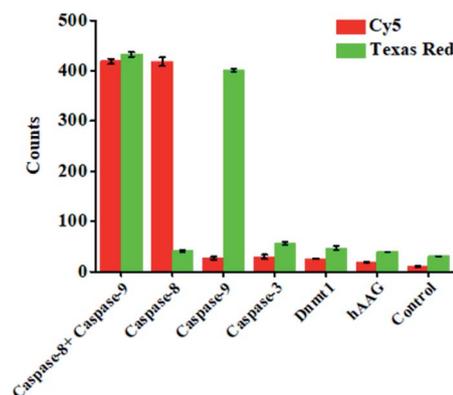

Fig. 4 Measurement of Cy5 counts and Texas Red counts in response to 0.025 U μL^{-1} caspase-8 + 0.025 U μL^{-1} caspase-9, 0.025 U μL^{-1} caspase-8, 0.025 U μL^{-1} caspase-9, 0.025 U μL^{-1} caspase-3, 0.025 U μL^{-1} Dnmt1, 0.025 U μL^{-1} hAAG, and the control with only reaction buffer. 0.5 U of Exo III was used in the experiments. Error bars represent the standard deviation of three experiments.
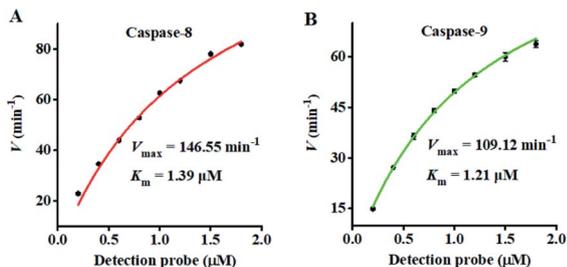
Fig. 5 Analysis of Michaelis–Menten kinetic parameters by the initial velocity method. (A) Variance of the initial velocity in response to various concentrations of detection probe 1. The caspase-8 concentration is 0.025 U μL^{-1}. (B) Variance of the initial velocity in response to various concentrations of detection probe 2. The caspase-9 concentration is 0.025 U μL^{-1}. The 0.5 U of Exo III was used in the experiments. Error bars represent the standard deviation of three experiments.

Fluoromethylketone (FMK),[72] chloromethylketone (CMK)[73] and difluorophenoxymethyl (OPh)[74] are competitive caspase inhibitors, and they can irreversibly inactivate caspases by forming a covalent thioether adduct with the cysteine of the active site in caspases. We used the caspase-8 inhibitor Z-IETD-FMK, caspase-9 inhibitor Ac-LEHD-CMK and broad-spectrum caspase inhibitor Q-VD-OPh as the model inhibitors to investigate the feasibility of the proposed nanosensor for the caspase inhibition assay. As shown in Fig. 6A, the relative activity of caspase-8 decreases with the increasing concentration of Z-IETD-FMK from 0 to 20 μM. The concentration of inhibitor required to reduce the activity of caspase-8 by 50% (IC$_{50}$) is

determined to be 1.95 μM, consistent with that obtained by the RCA-based fluorescence assay (0.9656 mM).[52] As shown in Fig. 6B, the relative activity of caspase-9 decreases with increasing concentration of Ac-LEHD-CMK from 0 to 300 nM. The IC$_{50}$ is determined to be 72.80 nM, consistent with the data from the manufacturer (70 nM). As shown in Fig. 6C and D, the relative activities of caspase-8 and caspase-9 decrease with increasing concentration of Q-VD-OPh, respectively. The IC$_{50}$ is determined to be 0.28 μM for caspase-8 and 0.31 μM for caspase-9. These results suggest that the proposed method can be applied for the screening of caspase inhibitors.

To demonstrate the feasibility of the proposed method for cellular caspase assays, we simultaneously measured endogenous caspase-8 and caspase-9 activity in a human cervical cancer cell line (HeLa cells), a human breast cancer cell line (MCF-7 cells), and a human acute T-lymphocytic leukemia cell line (Jurkat cells). Staurosporine (STS) is a broad-spectrum inhibitor of protein kinases with the capability of inducing *in vitro* apoptosis.[75] To avoid the interference from nonspecific caspases, we employed anti-caspase-8 and anti-caspase-9 antibodies to completely inhibit target caspase-8/9 activity (Fig. S6, ESI†), and calculated the specific caspase-8/9 signal ΔC according to eqn (1).

$$\Delta C = C - C_{a} \tag{1}$$

where C is the fluorescent count in the absence of antibody, and C_{a} is the fluorescent count in the presence of antibody. We first verified its capability of inducing apoptosis. In contrast to the low background signal in the control group without any cell extracts (Fig. 7A and B, black columns), distinct high ΔC_{Cy5} or $\Delta C_{Texas\ Red}$ is detected in the presence of HeLa cells (Fig. 7A and B, red columns), MCF-7 cells (Fig. 7A and B, blue columns) and Jurkat cells (Fig. 7A and B, magenta columns). After incubation with STS for 4 h, the caspase activities in the cell extracts were measured. STS can induce significantly enhanced ΔC_{Cy5} or
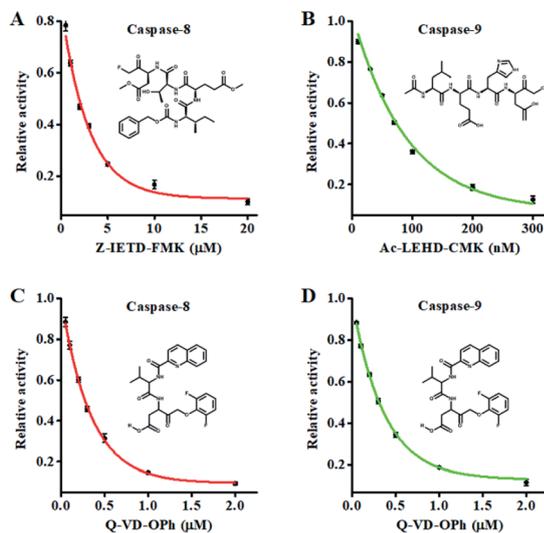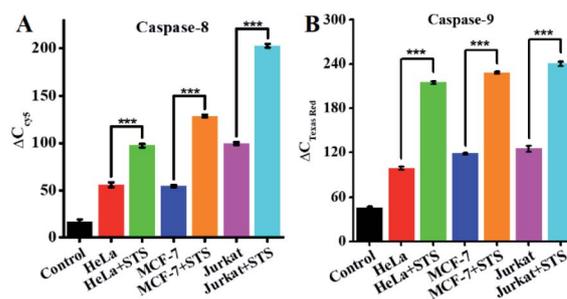

Fig. 6 (A) Variance of the relative activity of caspase-8 in response to different concentrations of Z-IETD-FMK. (B) Variance of the relative activity of caspase-9 in response to different concentrations of Ac-LEHD-CMK. (C) Variance of the relative activity of caspase-8 in response to different concentrations of Q-VD-OPh. (D) Variance of the relative activity of caspase-9 in response to different concentrations of Q-VD-OPh. The 0.025 U μL^{-1} caspase-8, 0.025 U μL^{-1} caspase-9 and 0.5 U of Exo III were used in the experiments. Error bars represent the standard deviation of three experiments.

Fig. 7 (A) Measurement of ΔC_{Cy5} in response to lysis (control, black column), HeLa cells (red column), HeLa cells + STS (green column), MCF-7 cells (blue column), MCF-7 cells + STS (orange column), Jurkat cells (magenta column), and Jurkat cells + STS (cyan column). The number of cells is 10 000. (B) Measurement of ΔC in response to lysis (control, black column), HeLa cells (red column), HeLa cells + STS (green column), MCF-7 cells (blue column), MCF-7 cells + STS (orange column), Jurkat cells (magenta column), and Jurkat cells + STS (cyan column). The number of cells is 10 000. Error bars represent the standard deviation of three experiments.

$\Delta C_{\text{Texas Red}}$ in HeLa cells (Fig. 7A and B, green columns), MCF-7 cells (Fig. 7A and B, orange columns) and Jurkat cells (Fig. 7A and B, cyan columns) compared to the cells without STS treatment (Student's t-test, $P < 0.001$), suggesting that the activation of caspases is involved in STS-induced apoptosis. These results demonstrate that the proposed nanosensor can be used for the sensitive detection of endogenous caspases activity.

Conclusions

In summary, we develop a sensitive nanosensor based on the integration of exonuclease III-powered 3D DNA walker with single-molecule detection for simultaneous measurement of initiator caspase-8 and caspase-9. The presence of caspase-8 and caspase-9 can induce the cleavage of peptides in two peptide–DNA detection probes, releasing two trigger DNAs from the magnetic beads. The two trigger DNAs can serve as the walker DNA to walk on the surface of signal probes@AuNPs powered by Exo III digestion, liberating numerous Cy5 and Texas Red fluorophores which can be quantified by single-molecule detection, with Cy5 indicating caspase-8 and Texas Red indicating caspase-9. This nanosensor possesses the following distinct advantages: (1) the introduction of the AuNP-based 3D DNA walker greatly reduces the background signal and amplifies the output signals, and the introduction of single-molecule detection further improves the detection sensitivity, endowing this nanosensor with higher sensitivity and less assay time than the reported caspase assays (Table S1, ESI†) and facilitating the accurate detection of low-abundant caspase with low sample consumption for biomedical research and disease diagnosis; (2) the amplification reaction can be conducted at constant temperature without the requirement of complicated thermal cycling, and the signal can be easily quantified by single-molecule counting; (3) the use of peptide–DNA detection probe-conjugated magnetic beads and signal probes@AuNPs greatly simplifies the experimental procedures, facilitating the simultaneous detection of multiple caspases. This nanosensor is very sensitive with a detection limit of 2.08×10^{-6} U μL^{-1} for caspase-8 and 1.71×10^{-6} U μL^{-1} for caspase-9, and it can be used for the simultaneous screening of caspase inhibitors and measurement of endogenous caspase activity in various cell lines at the single-cell level. Moreover, this nanosensor can be extended to detect various proteases by simply changing the peptide sequences of the detection probes.

Experimental section

Chemicals and materials

All oligonucleotides (Table 1) were HPLC-purified and synthesized by TaKaRa Bio Inc. (Dalian, China). The peptides were obtained from the Chinese Peptide Company (Hangzhou, China), and conjugated to DNA by TaKaRa Bio Inc. (Dalian, China). The caspase-8 (human, recombinant, active), caspase-9 (human, recombinant, active) and caspase-3 (human, recombinant, active) were obtained from Enzo Biochem, Inc. (Farmingdale, NY, USA). According to the datasheet from Enzo Biochem, Inc., the specific activity of caspase-8 is 5000 U mg^{-1} and its molecular weight is 55 391 g mol^{-1}, and thus 1 U μL^{-1} caspase-8 corresponds to 3.61 μM. Similarly, the specific activity of caspase-9 is 400 U mg^{-1} and its molecular weight is 46 281 g mol^{-1}, and thus 1 U μL^{-1} caspase-9 corresponds to 54.02 μM. Human DNA (cytosine-5)methyltransferase (Dnmt1), human alkyladenine DNA glycosylase (hAAG), exonuclease III (Exo III) and 10× CutSmart buffer were purchased from New England Biolabs (Ipswich, MA, USA). The streptavidin-coated magnetic beads (Dynabeads™ M-280 streptavidin), 1× phosphate buffered saline (1× PBS, pH 7.4) and SYBR gold were bought from Thermo Fisher Scientific (Waltham, MA, USA). The Au nanoparticles (10 nm, 0.01% Au) were bought from Nanocs, Inc. (New York, NY, USA). The caspase-8 inhibitor (Z-IETD-FMK) and caspase-9 inhibitor (Ac-LEHD-CMK) were obtained from Sigma-Aldrich (St. Louis, MO, USA). The broad-spectrum caspase inhibitor Q-VD-OPh was obtained from R&D System (Minneapolis, MN, USA). Staurosporine (STS) was purchased from Millipore Corporation (Billerica, MA, USA). Caspase-8 monoclonal antibody and caspase-9 monoclonal antibody were purchased from Proteintech Group Inc., (Chicago, IL, USA). Human cervical cancer cell line (HeLa cells), human breast cancer cell line (MCF-7 cells), and human acute T-lymphocytic leukemia cell line (Jurkat cells) were obtained from the cell bank of Chinese Academy of Sciences (Shanghai, China). All other reagents were of analytical grade and used as received without further purification. Ultrapure water obtained from a Millipore filtration system (Temecula, CA, USA) was used throughout all experiments.

Preparation of the detection probe-conjugated MBs

The assembly of detection probes onto the MBs was carried out according to the protocol of the manufacturer. 50 μL of the

Table 1 Sequences of the DNA oligonucleotides and peptide–DNA

Note	Sequence (5′–3′)
Detection probe 1	Biotin–(COOH)–Lys–Ser–His–Ser–His–Gly–Asp–Thr–Glu–Ile–Cys–(NH$_2$)–TTT TTC ACT TGA GGC TAA CAC TTT TT
Detection probe 2	Biotin–(COOH)–Lys–Arg–Gly–Arg–Gly–Gly–Asp–His–Glu–Leu–Cys(NH$_2$)--TTT TTC ACA ATC GGA CTA TCG TTT TT
Cleaved peptide–DNA 1	Asp–Thr–Glu–Ile–Cys-TTT TT C ACT TGA GGC TAA CAC TTT TT
Cleaved peptide–DNA 2	Asp–His–Glu–Leu–Cys-TTT TTC ACA ATC GGA CTA TCG TTT TT
Signal probe 1	SH-TTT TTT TTT TGT GTT AGC CTC AAG TG-Cy5
Signal probe 2	SH-TTT TTT TTT TCG ATA GTC CGA TTG TG-Texas Red

10 mg mL^{-1} streptavidin-coated MBs solution was washed three times using $1\times$ PBS. After resuspending with 50 μL of $1\times$ PBS, 10 μL of 10 μM detection probes were added to form the detection probes-MB nanostructure through biotin–streptavidin interaction at room temperature for 30 min. The detection probe-MBs were then washed five times using $1\times$ PBS to remove the uncoupled probes by magnetic separation, followed by resuspending in 50 μL of $1\times$ PBS.

Construction of signal probes@AuNPs

AuNPs (10 nm) were functionalized with thiolated signal probes using the freeze-directed methods.[76] The method is reagentless without the involvement of extra salts, acids, and surfactants. Specifically, 20 μL of 100 μM signal probes were mixed with 1 mL of AuNPs. The mixture was subsequently placed in a laboratory freezer at $-20\ °C$ for 2 h, followed by thawing at room temperature. At last, the signal probe-coated AuNPs were centrifuged and washed three times with ultrapure water to remove excess signal probes, and resuspended in 40 μL of sterile water, and stored at $4\ °C$. In the signal probes@AuNPs solution, the concentration of DNA was measured using a NanoDrop 2000c Spectrophotometer (Thermo Scientific, Wilmington, Delaware, USA) and the number of signal probes per AuNP is estimated to be 120 ± 1 for both Cy5-labeled signal probe 1 and Texas Red-labeled signal probe 2 (Fig. S2, ESI†).

Detection of caspase activities

The caspase activity assay includes two steps: (1) caspase-mediated cleavage of detection probes, and (2) recycling liberation of fluorophores induced by the Exo III-powered 3D DNA walker. The caspase-mediated cleavage of the detection probe was performed in 20 μL of solution containing 3.5 μL of $1\times$ PBS, 1 mM DTT, 8 μL of detection probe 1-conjugated MBs or/and detection probe 2-conjugated MBs, and 0.5 μL of caspase at different concentrations at $37\ °C$ for 1 h. After magnetic separation, the supernatant with cleavage products was collected for the next-step use. The Exo III-powered 3D DNA walker-based recycling liberation of fluorophores was performed in 20 μL of reaction solution containing $1\times$ CutSmart buffer (50 mM potassium acetate, 20 mM tris-acetate, 10 mM magnesium acetate, $100\ \text{μg mL}^{-1}$ BSA, pH 7.9), 0.71 μL of signal probe 1@AuNPs or/and 0.36 μL of signal probe 2@AuNPs, and 0.5 U of Exo III at $37\ °C$ for 1 h.

Ensemble fluorescence measurement

The 20 μL of reaction products was diluted to a final volume of 50 μL with ultrapure water for the measurement of fluorescence emission spectra using a 1 cm path length quartz cuvette on a Hitachi F-7000 fluorescence spectrophotometer (Tokyo, Japan). The excitation wavelength was 645 nm for Cy5 and 560 nm for Texas Red, and the emission spectra were recorded in the wavelength range of 660–750 nm for Cy5 and 600–680 nm for Texas Red with a slit width of 5 nm for both excitation and emission.

Single-molecule detection and data analysis

The reaction products of caspase-8 were diluted 200-fold in the imaging buffer (1 mg mL^{-1} glucose oxidase, 0.4% (w/v) D-glucose, 0.04% mg mL^{-1} catalase, 50 μg mL^{-1} BSA, 67 mM glycine-potassium hydroxide, 1 mg mL^{-1} Trolox, 2.5 mM magnesium chloride, pH 9.4), and the reaction products of caspase-9 were diluted 500-fold in the imaging buffer. For total internal reflection fluorescence (TIRF) imaging, 10 μL of the sample was directly pipetted onto the coverslips. The Cy5 and Texas Red fluorescent molecules were excited by the sapphire 640 and 561 nm lasers (Coherent, USA), respectively. The resulting photons were collected by an oil immersion objective (CFI Apochromat TIRF 100×). The Cy5 and Texas Red fluorescence signals were imaged on an Andor ixon Ultra 897 EMCCD camera (Andor, Belfast, UK) with an exposure time of 500 ms. For data analysis, the ImageJ software was used for counting the Cy5 and Texas Red fluorescent molecules from an imaging region of 600 × 600 pixels.

Gel electrophoresis

The reaction products were analyzed by 12% nondenaturing polyacrylamide gel electrophoresis (PAGE) in $1\times$ TBE buffer (9 mM Tris–HCl, 9 mM boric acid, 0.2 mM ethylenediaminetetraacetic acid, EDTA, pH 7.9) at a 110 V constant voltage at room temperature for 50 min. The gels were stained by SYBR gold and analyzed by a Bio-Rad ChemiDoc MP Imaging System (Hercules, CA, USA).

Kinetic analysis

To evaluate the enzyme kinetic parameters of caspases, we measured the initial velocity in the presence of 0.025 U μL^{-1} caspase (caspase-8 or caspase-9) and different concentrations of the detection probes at $37\ °C$ for 5 min. The kinetic parameter is fitted to the Michaelis–Menten equation.

$$V = \frac{V_{\max}[\text{S}]}{K_{\text{m}} + [\text{S}]} \qquad (2)$$

where $V_{\max}$ is the maximum initial velocity, [S] is the concentration of the detection probe, and K_{m} is the Michaelis–Menten constant.

Inhibition assay

To evaluate the effect of inhibitor upon the caspase activity, different concentrations of the inhibitor (Z-IETD-FMK for caspase-8, Ac-LEHD-CMK for caspase-9, and broad-spectrum caspase inhibitor Q-VD-OPh for both caspase-8 and caspase-9) were preincubated with 0.025 U μL^{-1} caspase (caspase-8 or caspase-9) at room temperature for 15 min, respectively. Then 8 μL of detection probe 1-conjugated MBs or detection probe 2-conjugated MBs were added into the mixture, and the reaction volume was adjusted to 20 μL with $1\times$ PBS, followed by the same detection procedure as described above. The relative activity (RA) of caspase was measured according to eqn (3).

$$\text{RA} = \frac{N_{\text{i}} - N_0}{N_{\text{t}} - N_0} \times 100\% \qquad (3)$$

where N_0 represents the Cy5 counts in the absence of caspase-8 or the Texas Red counts in the absence of caspase-9; N_t represents the Cy5 counts in the presence of caspase-8 (0.025 U μL^{-1}) or the Texas Red counts in the presence of caspase-9 (0.025 U μL^{-1}); and N_i represents the Cy5 counts in the presence of caspase-8 (0.025 U μL^{-1}) + inhibitor or the Texas Red counts in the presence of caspase-9 (0.025 U μL^{-1}) + inhibitor. The IC_{50} value was calculated from the curve of RA *versus* the inhibitor concentration.

Cell culture and preparation of cell extracts

HeLa cells and MCF-7 cells were cultured in Dulbecco's Modified Eagle's Medium (DMEM, Life Technologies, USA) with 10% FBS (Life Technologies, USA) and 1% penicillin–streptomycin (Gibco, USA). Jurkat cell was cultured in 1640 cell medium (Life Technologies, USA) with 10% FBS (Life Technologies, USA) and 1% penicillin–streptomycin (Gibco, USA). The cells were cultured at 37 °C in a humidified atmosphere containing 5% CO_2. For real sample analysis, cells in the exponential phase of growth were collected and counted using Countstar BioTech Automated Cell Counter IC1000 (Shanghai, China), washed twice with ice-cold 1× PBS, and centrifuged at 800 rpm for 5 min. To isolate cytoplasmic components from nuclear ones, the cells were treated with a nuclear protein extraction kit (Beyotime Biotechnology, Wuhan, China) and centrifuged at 3400 rpm for 15 min at 4 °C. For STS-induced apoptosis analysis, cells were incubated in 5 mL of cell medium containing 0.4 μM STS for 4 h prior to the cell lysis procedure. The protein concentration was measured using a NanoDrop 2000c Spectrophotometer (Thermo Scientific, Wilmington, Delaware, USA).

Author contributions

Meng Liu: conceptualization, methodology, investigation, writing – original draft preparation; Rui Xu: methodology, investigation; Wenjing Liu: conceptualization, writing – review and editing; Jian-Ge Qiu: conceptualization, writing – review and editing; Yan Wang: conceptualization, writing – review and editing; Fei Ma: conceptualization, writing – review and editing; Chun-yang Zhang: conceptualization, funding acquisition, writing – review and editing.

Conflicts of interest

There are no conflicts to declare.

Acknowledgements

Notes and references

1 K. Lauber, S. G. Blumenthal, M. Waibel and S. Wesselborg, *Mol. Cell*, 2004, **14**, 277–287.

2 Y. Fuchs and H. Steller, *Nat. Rev. Mol. Cell Biol.*, 2015, **16**, 329–344.

3 S. Ghavami, M. Hashemi, S. R. Ande, B. Yeganeh, W. Xiao, M. Eshraghi, C. J. Bus, K. Kadkhoda, E. Wiechec, A. J. Halayko and M. Los, *J. Med. Genet.*, 2009, **46**, 497–510.

4 M. Kurokawa and S. Kornbluth, *Cell*, 2009, **138**, 838–854.

5 E. C. Rui, M. M. S. Maria, M. C. G. Paulo, J. A. R. Carlos, M. S. F. Duarte, M. X. Joana, M. Rui and M. P. R. Cecilia, *Curr. Pharm. Des.*, 2010, **16**, 2851–2864.

6 P. J. Barr and L. D. Tomei, *Bio/Technology*, 1994, **12**, 487–493.

7 C. Thompson, *Science*, 1995, **267**, 1456–1462.

8 D. Hanahan and R. A. Weinberg, *Cell*, 2000, **100**, 57–70.

9 C. Pop and G. S. Salvesen, *J. Biol. Chem.*, 2009, **284**, 21777–21781.

10 A. Ashkenazi and V. M. Dixit, *Science*, 1998, **281**, 1305–1308.

11 A. G. Porter and R. U. Jänicke, *Cell Death Differ.*, 1999, **6**, 99–104.

12 L. H. Russell, E. Mazzio, R. B. Badisa, Z.-P. Zhu, M. Agharahimi, E. T. Oriaku and C. B. Goodman, *Anticancer Res.*, 2012, **32**, 1595–1602.

13 X.-M. Sun, M. MacFarlane, J. Zhuang, B. B. Wolf, D. R. Green and G. M. Cohen, *J. Biol. Chem.*, 1999, **274**, 5053–5060.

14 S. Yasuhara, Y. Zhu, T. Matsui, N. Tipirneni, Y. Yasuhara, M. Kaneki, A. Rosenzweig and J. A. J. Martyn, *J. Histochem. Cytochem.*, 2003, **51**, 873–885.

15 J. Su, T. W. Rajapaksha, M. E. Peter and M. Mrksich, *Anal. Chem.*, 2006, **78**, 4945–4951.

16 Y. Yang, Y. Liang and C.-y. Zhang, *Anal. Chem.*, 2017, **89**, 4055–4061.

17 G. B. Kim and Y.-P. Kim, *Theranostics*, 2012, **2**, 127–138.

18 Q. Wen, X. Zhang, J. Cai and P.-H. Yang, *Analyst*, 2014, **139**, 2499–2506.

19 V. Gurtu, S. R. Kain and G. Zhang, *Anal. Biochem.*, 1997, **251**, 98–102.

20 R. Onuki, A. Nagasaki, H. Kawasaki, T. Baba, T. Q. P. Uyeda and K. Taira, *Proc. Natl. Acad. Sci. U. S. A.*, 2002, **99**, 14716–14721.

21 Y. Yuan, R. Zhang, X. Cheng, S. Xu and B. Liu, *Chem. Sci.*, 2016, **7**, 4245–4250.

22 C. Köhler, S. Orrenius and B. Zhivotovsky, *J. Immunol. Methods*, 2002, **265**, 97–110.

23 H. Qi, M. Li, M. Dong, S. Ruan, Q. Gao and C. Zhang, *Anal. Chem.*, 2014, **86**, 1372–1379.

24 A. S. Goryashchenko, M. G. Khrenova and A. P. Savitsky, *Methods Appl. Fluoresc.*, 2018, **6**, 022001.

25 P. Yin, H. Yan, X. G. Daniell, A. J. Turberfield and J. H. Reif, *Angew. Chem., Int. Ed.*, 2004, **43**, 4906–4911.

26 C. Jung, P. B. Allen and A. D. Ellington, *Nat. Nanotechnol.*, 2016, **11**, 157–163.

27 W. B. Sherman and N. C. Seeman, *Nano Lett.*, 2004, **4**, 1203–1207.

28 H. Brutzer, F. W. Schwarz and R. Seidel, *Nano Lett.*, 2012, **12**, 473–478.

29 M. Liu, J. Fu, C. Hejesen, Y. Yang, N. W. Woodbury, K. Gothelf, Y. Liu and H. Yan, *Nat. Commun.*, 2013, **4**, 2127.

30 J.-S. Shin and N. A. Pierce, *J. Am. Chem. Soc.*, 2004, **126**, 10834–10835.

31 F. Dannenberg, M. Kwiatkowska, C. Thachuk and A. J. Turberfield, *Nat. Comput.*, 2015, **14**, 195–211.

32 Y. He and D. R. Liu, *Nat. Nanotechnol.*, 2010, **5**, 778–782.

33 D. Wang, C. Vietz, T. Schröder, G. Acuna, B. Lalkens and P. Tinnefeld, *Nano Lett.*, 2017, **17**, 5368–5374.

34 D. Yao, S. Bhadra, E. Xiong, H. Liang, A. D. Ellington and C. Jung, *ACS Nano*, 2020, **14**, 4007–4013.

35 M. Xiao, X. Wang, L. Li and H. Pei, *Anal. Chem.*, 2019, **91**, 11253–11258.

36 Y. Chen, Y. Xiang, R. Yuan and Y. Chai, *Nanoscale*, 2015, **7**, 981–986.

37 S. Cai, M. Chen, M. Liu, W. He, Z. Liu, D. Wu, Y. Xia, H. Yang and J. Chen, *Biosens. Bioelectron.*, 2016, **85**, 184–189.

38 Y. Yang, M. A. Goetzfried, K. Hidaka, M. You, W. Tan, H. Sugiyama and M. Endo, *Nano Lett.*, 2015, **15**, 6672–6676.

39 H. Zhang, X. Xu and W. Jiang, *Chem. Sci.*, 2020, **11**, 7415–7423.

40 N. Li, M. Du, S. Tian, X. Ji and Z. He, *Anal. Bioanal. Chem.*, 2019, **411**, 4055–4061.

41 X. Peng, Z.-B. Wen, P. Yang, Y.-Q. Chai, W.-B. Liang and R. Yuan, *Anal. Chem.*, 2019, **91**, 14920–14926.

42 Z. Xu, L. Liao, Y. Chai, H. Wang and R. Yuan, *Anal. Chem.*, 2017, **89**, 8282–8287.

43 X. Li, Q. Qiu, X. Ni, M. N. Hossain, X. Chen, H. Huang and H.-B. Kraatz, *Sens. Actuators B Chem.*, 2020, **319**, 128327.

44 C. Zhou, X. Duan and N. Liu, *Nat. Commun.*, 2015, **6**, 1–6.

45 H. Zhang, M. Lai, A. Zuehlke, H. Peng, X.-F. Li and X. C. Le, *Angew. Chem., Int. Ed.*, 2015, **54**, 14326–14330.

46 Y. Li, G. A. Wang, S. D. Mason, X. Yang, Z. Yu, Y. Tang and F. Li, *Chem. Sci.*, 2018, **9**, 6434–6439.

47 X. Qu, D. Zhu, G. Yao, S. Su, J. Chao, H. Liu, X. Zuo, L. Wang, J. Shi, L. Wang, W. Huang, H. Pei and C. Fan, *Angew. Chem., Int. Ed.*, 2017, **56**, 1855–1858.

48 E. Xiong, D. Zhen, L. Jiang and X. Zhou, *Anal. Chem.*, 2019, **91**, 15317–15324.

49 W. Li, L. Wang and W. Jiang, *Chem. Commun.*, 2017, **53**, 5527–5530.

50 S. D. Mason, Y. Tang, Y. Li, X. Xie and F. Li, *TrAC, Trends Anal. Chem.*, 2018, **107**, 212–221.

51 Z. Xu, Y. Chang, Y. Chai, H. Wang and R. Yuan, *Anal. Chem.*, 2019, **91**, 4883–4888.

52 M. Liu, D. Zhang, X. Zhang, Q. Xu, F. Ma and C.-y. Zhang, *Chem. Commun.*, 2020, **56**, 5243–5246.

53 X. Zuo, F. Xia, Y. Xiao and K. W. Plaxco, *J. Am. Chem. Soc.*, 2010, **132**, 1816–1818.

54 J. Kim and C. J. Easley, *Bioanalysis*, 2011, **3**, 227–239.

55 G. T. Walker, M. S. Fraiser, J. L. Schram, M. C. Little, J. G. Nadeau and D. P. Malinowski, *Nucleic Acids Res.*, 1992, **20**, 1691–1696.

56 F. Ma, Y. Yang and C.-y. Zhang, *Anal. Chem.*, 2014, **86**, 6006–6011.

57 M. M. Ali, F. Li, Z. Zhang, K. Zhang, D.-K. Kang, J. A. Ankrum, X. C. Le and W. Zhao, *Chem. Soc. Rev.*, 2014, **43**, 3324–3341.

58 T. Notomi, H. Okayama, H. Masubuchi, T. Yonekawa, K. Watanabe, N. Amino and T. Hase, *Nucleic Acids Res.*, 2000, **28**, e63.

59 F. Ma, Y. Li, B. Tang and C.-y. Zhang, *Acc. Chem. Res.*, 2016, **49**, 1722–1730.

60 C.-c. Li, H.-y. Chen, J. Hu and C.-y. Zhang, *Chem. Sci.*, 2020, **11**, 5724–5734.

61 M.-Y. Li, Y.-Q. Wang, Y.-L. Ying and Y.-T. Long, *Chem. Sci.*, 2019, **10**, 10400–10404.

62 L.-J. Wang, X. Han, J.-G. Qiu, B. Jiang and C.-Y. Zhang, *Chem. Sci.*, 2020, **11**, 9675–9684.

63 W. Ma, H. Ma, J.-F. Chen, Y.-Y. Peng, Z.-Y. Yang, H.-F. Wang, Y.-L. Ying, H. Tian and Y.-T. Long, *Chem. Sci.*, 2017, **8**, 1854–1861.

64 Z.-y. Wang, L.-j. Wang, Q. Zhang, B. Tang and C.-y. Zhang, *Chem. Sci.*, 2018, **9**, 1330–1338.

65 Z. Ye, H. Liu, F. Wang, X. Wang, L. Wei and L. Xiao, *Chem. Sci.*, 2019, **10**, 1351–1359.

66 Y. Xie, R. Zhao, Y. Tan, X. Zhang, F. Liu, Y. Jiang and C. Tan, *ACS Appl. Mater. Interfaces*, 2012, **4**, 405–410.

67 M. S. Rahman, T. Kabashima, H. Yasmin, T. Shibata and M. Kai, *Anal. Biochem.*, 2013, **433**, 79–85.

68 L. Liu, H. Zhang, Z. Wang and D. Song, *Biosens. Bioelectron.*, 2019, **141**, 111403.

69 Z.-y. Wang, P. Li, L. Cui, Q. Xu and C.-y. Zhang, *Anal. Chem.*, 2020, **92**, 13573–13580.

70 C.-c. Li, W.-x. Liu, J. Hu and C.-y. Zhang, *Chem. Sci.*, 2019, **10**, 8675–8684.

71 X. Liu, X. Song, D. Luan, B. Hu, K. Xu and B. Tang, *Anal. Chem.*, 2019, **91**, 5994–6002.

72 C. J. F. Van Noorden, *Acta Histochem.*, 2001, **103**, 241–251.

73 H. Fauvel, P. Marchetti, C. Chopin, P. Formstecher and R. Nevière, *Am. J. Physiol. Heart Circ. Physiol.*, 2001, **280**, H1608–H1614.

74 K. Kuželová, D. Grebeňová and B. Brodská, *J. Cell. Biochem.*, 2011, **112**, 3334–3342.

75 G. Feng and N. Kaplowitz, *Am. J. Physiol. Gastrointest. Liver Physiol.*, 2002, **282**, G825–G834.

76 B. Liu and J. Liu, *J. Am. Chem. Soc.*, 2017, **139**, 9471–9474.